Stroke

CLINICAL AND POPULATION SCIENCES

Dynamic Imaging of Blood Coagulation Within the Hematoma of Patients With Acute Hemorrhagic Stroke

Muhammad E. Haque, PhD; Seth B. Boren, MS; James Mills, MS; Kerry G. Schneider, BS; Maria Parekh, MD; Stuart M. Fraser, MD; Ivo Bach, MD; Praveen Hariharan, MD; Pamela J. Zelnick, MD; Felix S. Guerra Castanon, MD; Asim Naveed, MD; Muhammad Tariq, MD; Octavio D. Arevalo, MD; Khader M. Hasan, PhD; Miguel Escobar, MD; Xiurong Zhao, MD; Clark Sitton, MD; Ponnada A. Narayana, PhD; James C. Grotta, MD; Jaroslaw Aronowski, PhD; Sean I. Savitz, MD

BACKGROUND: The dynamics of blood clot (combination of Hb [hemoglobin], fibrin, and a higher concentration of aggregated red blood cells) formation within the hematoma of an intracerebral hemorrhage is not well understood. A quantitative neuroimaging method of localized coagulated blood volume/distribution within the hematoma might improve clinical decision-making.

METHODS: The deoxyhemoglobin of aggregated red blood cells within extravasated blood exhibits a higher magnetic susceptibility due to unpaired heme iron electrons. We propose that coagulated blood, with higher aggregated red blood cell content, will exhibit (1) a higher positive susceptibility than noncoagulated blood and (2) increase in fibrin polymerization–restricted localized diffusion, which can be measured noninvasively using quantitative susceptibility mapping and diffusion tensor imaging. In this serial magnetic resonance imaging study, we enrolled 24 patients with acute intracerebral hemorrhage between October 2021 to May 2022 at a stroke center. Patients were 30 to 70 years of age and had a hematoma volume >15 cm^3 and National Institutes of Health Stroke Scale score >1. The patients underwent imaging 3×: within 12 to 24 (T1), 36 to 48 (T2), and 60 to 72 (T3) hours of last seen well on a 3T magnetic resonance imaging system. Three-dimensional anatomic, multigradient echo and 2-dimensional diffusion tensor images were obtained. Hematoma and edema volumes were calculated, and the distribution of coagulation was measured by dynamic changes in the susceptibilities and fractional anisotropy within the hematoma.

RESULTS: Using a coagulated blood phantom, we demonstrated a linear relationship between the percentage coagulation and susceptibility (R^2=0.91) with a positive red blood cell stain of the clot. The quantitative susceptibility maps showed a significant increase in hematoma susceptibility (T1, 0.29±0.04 parts per millions; T2, 0.36±0.04 parts per millions; T3, 0.45±0.04 parts per millions; P<0.0001). A concomitant increase in fractional anisotropy was also observed with time (T1, 0.40±0.02; T2, 0.45±0.02; T3, 0.47±0.02; P<0.05).

CONCLUSIONS: This quantitative neuroimaging study of coagulation within the hematoma has the potential to improve patient management, such as safe resumption of anticoagulants, the need for reversal agents, the administration of alteplase to resolve the clot, and the need for surgery.

GRAPHIC ABSTRACT: A graphic abstract is available for this article.

Key Words: blood coagulation ■ cerebral hemorrhage ■ fibrin ■ magnetic resonance imaging ■ quantitative phase imaging

Correspondence to: Muhammad E. Haque, PhD, McGovern Medical School, The University of Texas Health Science Center at Houston (UTHealth), 6431 Fannin St, Houston, TX 77030. Email muhammad.e.haque@uth.tmc.edu

Supplemental Material is available at https://www.ahajournals.org/doi/suppl/10.1161/STROKEAHA.123.044343.

For Sources of Funding and Disclosures, see page 1023.

Nonstandard Abbreviations and Acronyms

$CaCl_2$	calcium chloride
CT	computed tomography
FA	fractional anisotropy
FM	Fugl-Meyer
Hb	hemoglobin
HCT	homologous contralesional tissues
HE	hematoma expansion
ICH	intracerebral hemorrhage
LMER	linear mixed effects regression
MD	mean diffusivity
MRI	magnetic resonance imaging
NIHSS	National Institutes of Health Stroke Scale
PHE	perihematomal edema
QSM	quantitative susceptibility mapping
RBC	red blood cell
tPA	tissue-type plasminogen activator

The rate of blood coagulation plays a critical role in intracerebral hemorrhage (ICH). ICH causes brain injury directly by tissue compression and mass effect. The components of extravasated blood also pose injury to surrounding tissue.[1–5] Beyond direct cellular injury, perihematomal edema (PHE) also causes tissue compression.[1,6–9] Animal studies have demonstrated that the formation of a blood clot within the hematoma is directly linked to the formation of cerebral edema.[10–13] Thus, there is a dynamic interaction involving coagulation. On the one hand, nonclotted blood results in less pronounced edema and thus a potentially better outcome. On the other hand, noncoagulated blood may lead to hematoma expansion (HE) that can worsen outcomes.[10] Both computed tomography (CT) and magnetic resonance imaging (MRI) scans are routinely used in the evaluation of hematoma location, size, and PHE expansion but have not been used to evaluate clot formation within the hematoma. The ability to evaluate clot formation in ICH could accelerate clinical intervention in these patients.

Recent progress in quantitative susceptibility mapping (QSM)—an advanced MRI image-processing technique—enabled accurate estimation of iron-induced magnetic susceptibility (χ).[14–16] A blood clot is a combination of aggregated red blood cells (RBCs), Hb (hemoglobin), fibrin, platelets, hemosiderin, leukocytes, platelets, and other damage-associated cellular debris.[17,18] After RBC lysis, the heme iron oxidation state changes from oxyhemoglobin to deoxyhemoglobin followed by an intracellular or extracellular methemoglobin, and finally, hemosiderin results in a dynamic signal heterogeneity as hematoma evolves.[19–21] The unpaired iron electrons present in an aggregated RBC's deoxyhemoglobin induce magnetic susceptibility. Therefore, a region with a higher number of aggregated deoxyhemoglobin molecules of the retracted clot will exhibit a higher positive susceptibility in comparison to the regions with fewer deoxyhemoglobin molecules. We hypothesized that coagulated blood exhibits a higher positive susceptibility than liquid blood within the hematoma and the surrounding PHE (which is made of predominantly a diamagnetic water molecule) exhibits negative susceptibility. Furthermore, voxels with coagulated blood will increase localized diffusion hindrance that is consistent with increase in susceptibility. Previously, both in vivo and in vitro imaging of hematoma and animal blood clot phantom has reported a significantly higher susceptibility.[22–25] In this prospective serial MRI study, we aimed to evaluate the progression of coagulation within the hematomas of patients with acute ICH to develop a noninvasive imaging biomarker for coagulopathy.

METHODS

Human Subject Study Institutional Review Board Compliance

The study was approved by the institutional review board of the University of Texas Health Sciences Center at Houston and by the Memorial Hermann Hospital Office of Research. Written informed consent was obtained after a thorough discussion with patients and family members. All methods comply with the approved study protocol.

Data Availability Statement

Anonymized serial imaging and clinical data used in this study are available from the corresponding author upon request.

Patient Enrollment and Human Protection

The study was approved by the institutional review board of the Memorial Hermann Hospital Office of Research and the University of Texas Health Sciences Center at Houston. Twenty-four patients with acute spontaneous ICH admitted to the Memorial Hermann Hospital-Texas Medical Center between October 2021 and May 2022 were enrolled after a thorough discussion with patients and family members, and written informed consents were obtained. The patient's inclusion and exclusion criteria are described in the Supplemental Material, and the recruitment flowchart is summarized in Figure S1.

Blood Phantom Imaging

We collected 100 mL of fresh human blood from a healthy volunteer and prepared 3 phantoms (2 blood and 1 plasma). Blood was transferred into two 50-mL Falcon tubes with 3.2% sodium citrate solution as an anticoagulant, and samples were centrifuged at 550*g* for 15 minutes. A mixture of hematocrit with citrated plasma at the ratio of 7:3 corresponding to 70% hematocrit was produced in 2 different tubes with 20 mL solid agarose gel at the base of each tube. An additional 50-mL tube contains 20 mL of plasma only. Coagulation was initiated using

 Stroke. 2024;55:1015–1024. DOI: 10.1161/STROKEAHA.123.044343

2.06% calcium chloride ($CaCl_2$). Only 1 blood and plasma tube was coagulated, and a water phantom was used as a control. The phantoms were imaged, and susceptibility maps were created. We also obtained human blood from the blood bank and prepared five 50-mL blood clot phantoms with 80%, 60%, 40%, 20%, and 10% of RBC, respectively. The phantoms were imaged, and susceptibility was measured using a region of interest. A linear association between the %RBC and susceptibility was statistically tested.

After imaging, the blood and plasma clots were removed from the tube and placed in 10% formalin for 24 hours and then embedded in paraffin. The clot was cut into 5 slices with 3-µm thickness and stained with Martius Scarlet Blue and hematoxylin and eosin as described previously.[26,27] The slides were scanned at the resolution of 0.25 µm per pixel using the MoticEasyScan scanner.

Neurological and Radiological Assessments

All participants were imaged 3× within 12 to 24 (T1), 36 to 48 (T2), and 60 to 72 (T3) hours of last seen well. Diagnostic CT images were performed within 30 to 60 minutes of arrival at the hospital as part of the standard-of-care protocols followed by the first study-related MRI within 12 to 24 hours. All baseline (at the time of admission) neurological and clinical assessments were obtained via medical records that included blood pressure management, reversal of anticoagulant, international normalized ratio, Glasgow Coma Scale, National Institutes of Health Stroke Scale (NIHSS), and radiology diagnostic reports. Additional research assessment included serial Fugl-Meyer (FM) upper extremity and NIHSS whenever possible and a detailed qualitative radiological assessment that included a change in mass effects, midline shift, presence of ischemia, and tissue compression at each follow-up imaging time point.

Progression of Coagulation and Imaging Methodology

The rate of coagulation was assessed by measuring the change in susceptibility within the hematoma and PHE using QSM. This technique allows a clear delineation between iron (positive susceptibility) and water/cerebral spinal fluid (negative susceptibility); such a distinction is not possible using the change in transverse relaxation rate (also known as R2*). This is because QSM uses the phase information of the MRI signal to compute the susceptibility.

We also expected that the progression of coagulation would increase a hindrance in water molecular diffusion directionality. This change in diffusion hindrance can be calculated by the ratio of axial diffusivity/radial diffusivity, known as fractional anisotropy (FA) and an average of axial diffusivity and radial diffusivity (axial diffusivity+2×radial diffusivity)/3 known as mean diffusivity (MD), the 2 commonly used diffusion tensor imaging metrics.[28]

MRI Imaging

Serial images were obtained on a 3.0T Philips Ingenia system (Philips Medical Systems, Best, the Netherlands). The image acquisition parameters, image processing steps, and creation of QSM are provided in the Supplemental Material. Figure 1 shows a flowchart of image processing steps used to measure the hematoma and PHE volumes, χ, FA, and MD. The image processing steps involved to create QSM are presented in Figure S2.

Lesion Volume Measurements and Region of Interest

The Analyze 12.0 software (Analyze Direct, Inc, KS) was used to delineate and compute hematoma and PHE volumes on fluid attenuation inversion recovery images at all 3 time points.

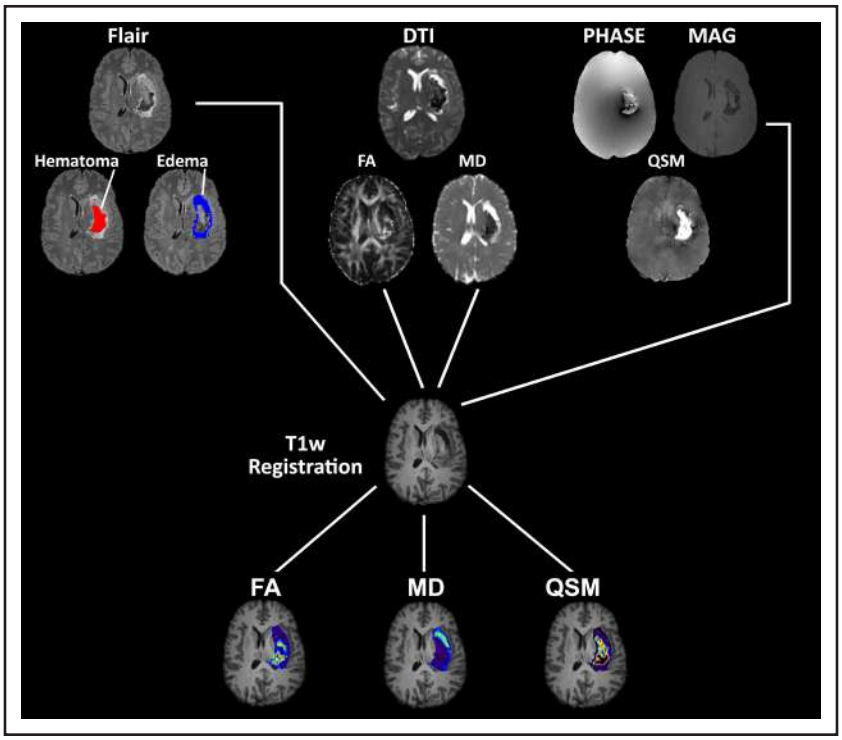

Figure 1. Summary of image processing steps used to quantify the images.
The first row (**left** to **right**) is fluid attenuation inversion recovery (FLAIR) b0 of diffusion tensor imaging (DTI), and phase and magnitude (MAG) image of multigradient echo. The second row shows the segmented hematoma, edema, and processed fractional anisotropy (FA), mean diffusivity (MD), and quantitative susceptibility maps (QSMs). The third row shows the T1-weighted image (T1w) registration process to the parametric maps, segmented hematoma, perihematomal edema volumes, and matching contralesional homologous regions. The last row illustrates the FA, MD, and QSM values overlaid on a high-resolution anatomic image.

Briefly, a seed point was selected within the hematoma to create a hematoma mask. The same process was repeated to delineate the PHE mask. The 2 homologous contralesional tissues (HCTs) regions of interest are referred to as HCT and HCT2 for matching hematoma and PHE, respectively. The hematoma and PHE volume masks were saved and used as region of interest to compute χ, FA, and MD in both ipsilesional and contralesional hemispheres.

Statistical Analysis

Ipsilesional and contralesional susceptibility, FA, and MD values were compared using *t* tests at the first time point (T1). The primary analysis to examine change over time was conducted using linear mixed effects regression (LMER).[29] The imaging and clinical outcomes of interest were analyzed separately in LMER models adjusting for age, sex, and first MRI time. The time metric in the analysis was time point (T1, T2, and T3), treated as a categorical variable. Adjusted means were estimated at each time point, and differences in means for T2 and T3 from T1 were assessed. Exploratory LMER analyses were conducted to examine the relationship between imaging and clinical (Glasgow Coma Scale, NIHSS, FM upper extremity) measures, again adjusting for age, sex, and time at hospital admission but now using duration as the time metric. Some measures were time invariant (ie, collected only at the first visit), and their longitudinal effects are estimated from the interaction with duration. Some covariates were time varying in the LMER model (ie, collected at all visits). These covariates were partitioned into between- and within-subject effects, and the parameters for the 2 effects are the cross-sectional and longitudinal estimates associated with the clinical outcomes, respectively.[30] Consequently, the key predictors in these models were the interactions of the time-invariant covariates with duration or the cross-sectional and longitudinal components of the time-varying covariates. In all LMER models, random intercept terms were specified for participants, and maximum likelihood methods were used for estimation, yielding unbiased estimates under the assumption that the missing data mechanism is ignorable.[31]

RESULTS

Demographics and Clinical Information

Twenty-four patients (14 men and 10 women) with an average age of 65.8±12.4 years with acute ICH were serially imaged with a median time of 18.7 (T1), 45.6 (T2), and 70.5 (T3) hours of last seen well. Nineteen patients completed all 3 imaging time points, 1 patient completed 2 time points, and 4 patients were imaged only at the first time point. Two patients died after the first imaging session. The median baseline Glasgow Coma Scale and NIHSS scores were 14 (interquartile range, 10.5–15.0) and 11 (interquartile range, 6.5–18.5), respectively. All patients had hypertensive or anticoagulant-related cerebral hemorrhage with a median baseline blood pressure of 170/87 (interquartile range, 150/79 to 190/101) mm Hg. Twelve patients had a variable amount of blood extended to the lateral ventricles. All patients exhibited mass effect with 63% having the involvement of the corticospinal tract and 46% having midline shift (4 [interquartile range, 3.0–4.5] mm) measured at the level of septum pellucidum. The baseline clinical profiles are summarized in the Table.

Blood Phantom Susceptibilities

Figure 2 illustrates qualitative and histological analyses of human blood clots. Figure 2A shows a T2*-weighted contrast demonstrating distinct spots of hyperintense and hypointense signal in a coagulated blood tube (with $CaCl_2$), whereas a noncoagulated blood tube (without $CaCl_2$) illustrates homogenous signal attenuation. Figure 2B illustrates the corresponding susceptibility maps of each tube. The coagulated blood shows spots with higher susceptibility as compared with the noncoagulated blood. Both the water and plasma tubes exhibited negative susceptibility despite one being liquid (water) and the other being solid (plasma). Figure 2C and 2D shows a histological analysis of the blood and plasma

Table. A Summary of the Patient's Demographic and Clinical Assessments

Demographic and baseline parameters	Clinical profile
No. of patients enrolled	24
Patients completed all imaging	19 (79%)
Sex	Male, 14 (58%); female, 10 (42%)
Age, y	65.8±12.4
Laterality	Left, 11 (45%); right, 13 (54%)
Patients on antithrombotic	7 (29%; plavix, 3; aspirin, 3; eliquis, 1)
Baseline median GCS	14 (IQR, 10.5–15)
Baseline median NIHSS	11 (IQR, 6.5–18)
Baseline median diastolic/systolic BP, mm Hg	170/87 (IQR, 150/79–190/101)
Median MRI time (from last seen well), h	
First MRI	18.7 (IQR, 13.3–28.2)
Second MRI	45.6 (IQR, 35.7–52.0)
Third MRI	70.5 (IQR, 61.0–78.6)
Radiological assessment	
Baseline (CT) median hematoma volume, cm^3	23.3±17
Location	BG, 37%; thalamus, 33%; FL, 16%; BG+thalamus, 8%; other, 8%
Median midline shift	11 (46%); 4.0 (IQR, 3–4.5) mm
Mass effect	24 (100%)
CST effect	15 (63%)
Presence of ischemia (first MRI)	4 (17%)

BG indicates basal ganglia; BP, blood pressure; CST, corticospinal tract; CT, computed tomography; FL, frontal lobe; GCS, Glasgow Coma Scale; IQR, interquartile range; MRI, magnetic resonance imaging; and NIHSS, National Institutes of Health Stroke Scale.

Stroke. 2024;55:1015–1024. DOI: 10.1161/STROKEAHA.123.044343

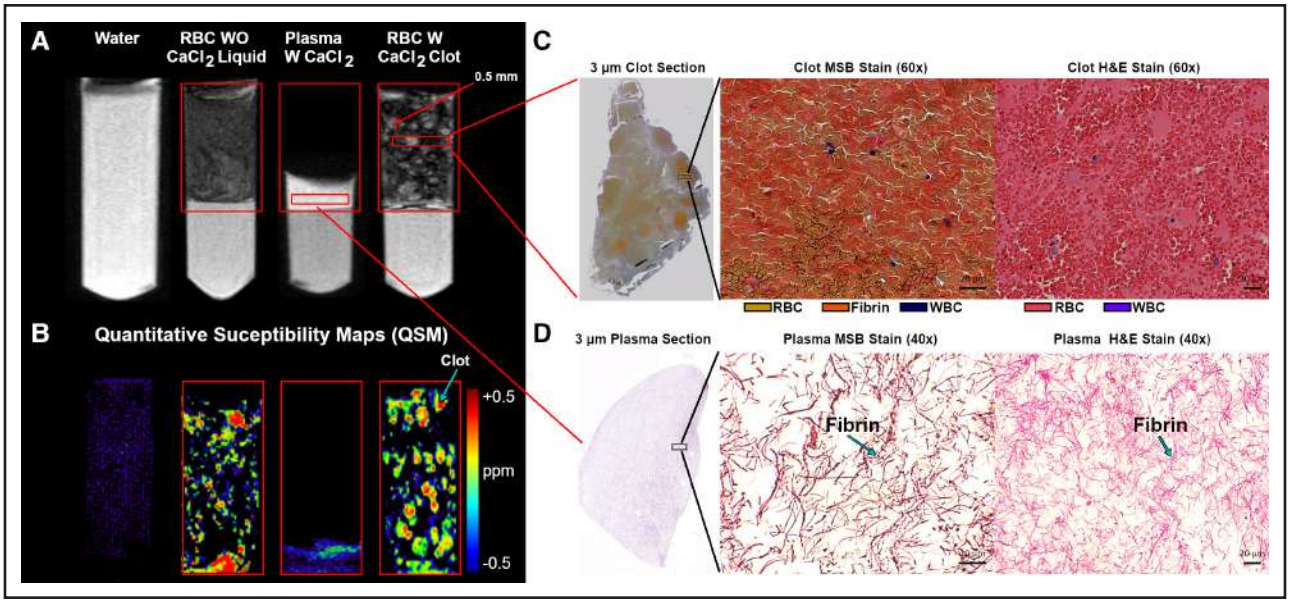

Figure 2. Qualitative and quantitative analysis of human blood clots.
A, T2*-weighted MRI signal contrast in (**left** to **right**) water, 70% red blood cells without (RBC WO) calcium chloride ($CaCl_2$) liquid blood, coagulated plasma with $CaCl_2$, and 70% red blood cells with (RBC W) $CaCl_2$ (coagulated blood), respectively. **B**, **Left** to **Right**, The corresponding quantitative susceptibility map of the tubes in **A**. Coagulated blood showed pockets of clotted blood distributed throughout the tube with higher susceptibility. **C**, A 3-µm slice of coagulated blood with Martius Scarlet Blue (MSB)–stained displayed pockets of clots randomly distributed as seen in MRI. A high-resolution (60×) image of the clot with MSB stain (**C**, **middle**) showed the presence of fibrin (red), red blood cells (RBCs; yellow), and white blood cells (WBCs; blue), whereas hematoxylin and eosin (H&E; **C**, **right**) only showed the RBC and WBC. The coagulated plasma with no RBC (**D**, **left** to **right**) illustrates a 3-µm slice section with no pockets of clotted blood, a high-resolution (40×) MSB, and H&E stained with fibrin only. QSM indicates quantitative susceptibility mapping.

clots. A single 3-µm-thick slice of blood clot showing pockets of clots corresponds to high susceptibility on QSM. The Martius Scarlet Blue stain of the blood clot shows RBC (yellow) trapped in the fibrin web (red), whereas plasma clots just show the fibrin web. The corresponding hematoxylin and eosin stain of the clot shows RBCs (red) and WBCs (blue).

The linear relation between the clot's %RBC and susceptibility with R^2=0.914 is presented in the Supplemental Material. The FA and MD measurements also exhibited a positive and negative linear relation with the %RBC with R^2 of 0.79 and 0.94, respectively (Figure S3).

Hematoma and PHE Volume

The mean hematoma volume calculated from the standard-of-care CT scans using the ABC/2 method was 23.3±17.0 cm^3 without adjusting for age. The average adjusted hematoma volume measured via fluid attenuation inversion recovery MRI did not significantly change over time (T1, 18.9±3.1 cm^3; T2, 18.6±3.1 cm^3; T3, 18.4±3.1 cm^3; P=0.38). Hematomas exhibited a heterogeneous signal intensity depending on the heme iron oxidation state, cellular compartmentalization, and hematoma age. The PHE volume significantly increased over time (T1, 25.3±3.6 cm^3; T2, 28.1±3.7 cm^3; T3, 32.9±3.7 cm^3; P=0.019). There was a positive association between PHE and hematoma volumes (coefficient, 0.91; SE, 0.17; P<0.0001 [95% CI, 0.57–1.25]), that is, patients with larger hematoma had larger PHE while controlling for age. The evolution of hematoma and PHE is shown in Figure 3 (top row) and box plot. Figure 4Ai and 4Bi summarizes the temporal changes, respectively.

Rate of Coagulation (Magnetic Susceptibility)

QSMs show that the average hematoma susceptibility significantly increased over time (T1, 0.29±0.04 parts per millions [ppm]; T2, 0.36±0.04 ppm; T3, 0.45±0.04 ppm; P<0.0001). The average rate of coagulation (increase in susceptibility per hour) between T1 and T2 was 0.0025±0.0041 ppm/h, which increased to 0.0031±0.0043 ppm/h between T2 and T3. The overall rate of coagulation was 0.00290±0.0029 ppm/h. As compared with the hematoma, the HCTs exhibited significantly lower susceptibility (T1, 0.0027±0.0038; T2, 0.00049±0.0040; T3, 0.00019±0.0041; P<0.0001) at all 3 time points with no temporal changes over time (P=0.86).

The PHE tissues exhibited an increase in negative susceptibility (T1, −0.056±0.016 ppm; T2, −0.068±0.017 ppm; T3, −0.10±0.017 ppm; P=0.08) over time. In the HCTs (HCT2), the negative susceptibilities (T1, −0.0072±0.002 ppm; T2, −0.0091±0.003 ppm; T3, −0.0084±0.003 ppm) were lower than ipsilesional, but there was no significant difference between the 2 regions (P=0.30). The HCT2 exhibited no

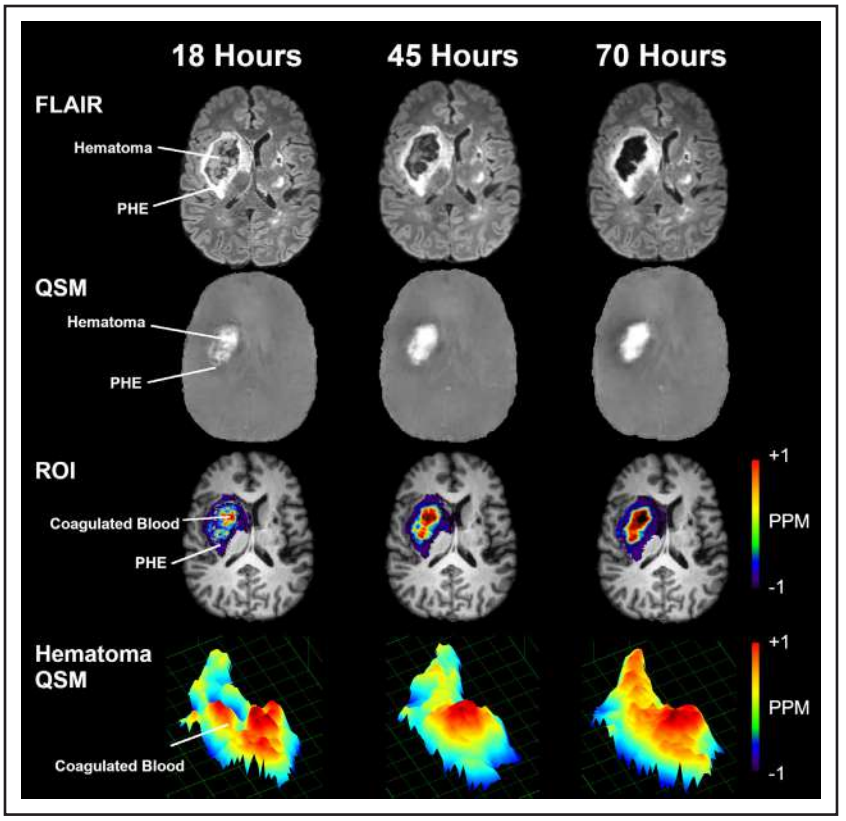

Figure 3. An illustration of the temporal coagulation within hematoma between hyperacute to acute stages on a representative patient with intracerebral hemorrhage.
The first row shows the change in contrast within the hematoma over time on a fluid attenuation inversion recovery (FLAIR) image. The second row displays quantitative susceptibility maps (QSMs) at 3 time intervals with a distinct increase in hypointense negative susceptibility in the surrounding perihematomal edema (PHE) at the last time point. The third row illustrates the change in susceptibilities within hematoma and PHE over time overlaid on a T1-weighted image. The last row is a zoomed hematoma volume showing the susceptibility gradient within the hematoma and changes over time. PPM indicates parts per millions; and ROI, region of interest.

significant susceptibility change over time (P=0.70). Figure 3 (second row) shows QSMs illustrating an increase in susceptibility within hematoma. The poor contrast in the susceptibility map is due to the ppm scaling window. Figure 3 (third row is hematoma susceptibility overlaid on a fluid attenuation inversion recovery, and fourth row is zoomed hematoma) also shows the spatial distribution of coagulation within the hematoma. Figure 4Aii and 4Bii is a box plot showing the difference and temporal change in susceptibility within the hematoma and PHE, respectively.

FA and MD

In parallel to hematoma susceptibility, the hematoma diffusion hindrance via change in directionality (increase in FA) was significantly (T1, 0.40±0.02; T2, 0.45±0.02; T3, 0.47±0.02; P=0.0086) increased over time. As compared with hematoma, the matching HCT exhibited significantly (T1, 0.27±0.01; T2, 0.26±0.01; T3, 0.27±0.01; P<0.0001) lesser diffusion hindrance (lower FA) at all 3 imaging time points and temporally remained unchanged (P=0.35). The surrounding PHE exhibited significantly lesser diffusion hindrance (FA: T1, 0.27±0.01; T2, 0.26±0.01; T3, 0.25±0.01) with no significant temporal changes either in the PHE (P=0.25) or matching HCT2 (P=0.85). Figure 4Aiii and 4Biii shows box plots illustrating the ipsilesional temporal FA variance within the hematoma and PHE, respectively.

The average MD in the hematoma at all 3 time points (T1, 676.4±37.0; T2, 730.6±39.1; T3, 750.1±39.6 $\times 10^{-6}$ mm^2/s) was significantly attenuated than the surrounding PHE (T1, 1013.0±30.1; T2, 982.2±30.8; T3, 1022.6±31.1 $\times 10^{-6}$ mm^2/s; P<0.0001). However, the matching contralesional region (HCT) exhibited significantly higher MD (P<0.0001) at all 3 time points. The matching contralesional (HCT2) PHE exhibited slightly elevated MD but no significant difference between ipsilesional and contralesional MDs. Temporally, both contralesional HCT and HCT2 showed no significant change in MD with a P value of 0.068 and 0.36, respectively. Figure 4Aiv and 4Biv is a box plot illustrating the ipsilesional MD variance within hematoma and PHE over time, respectively. All the quantifications at each time point are summarized in Table S1.

Association Between Clinical Assessment and Imaging Metrics

There was a significant association between the positive hematomal susceptibility and hematoma volume (coefficient, −0.0069; SE, 0.0030; P=0.025 [95% CI, −0.0130 to −0.0009]) and a weak association (coefficient, 0.0030; SE, 0.0016; P=0.069 [95% CI, −0.00025 to −0.0062]) with the PHE volume. The NIHSS was strongly associated with both the hematoma (coefficient, 1.24; SE, 0.45; P=0.0097 [95% CI, 0.32–2.16]) and PHE (coefficient, 1.40; SE, 0.49; P=0.0077 [95% CI,

 Stroke. 2024;55:1015–1024. DOI: 10.1161/STROKEAHA.123.044343

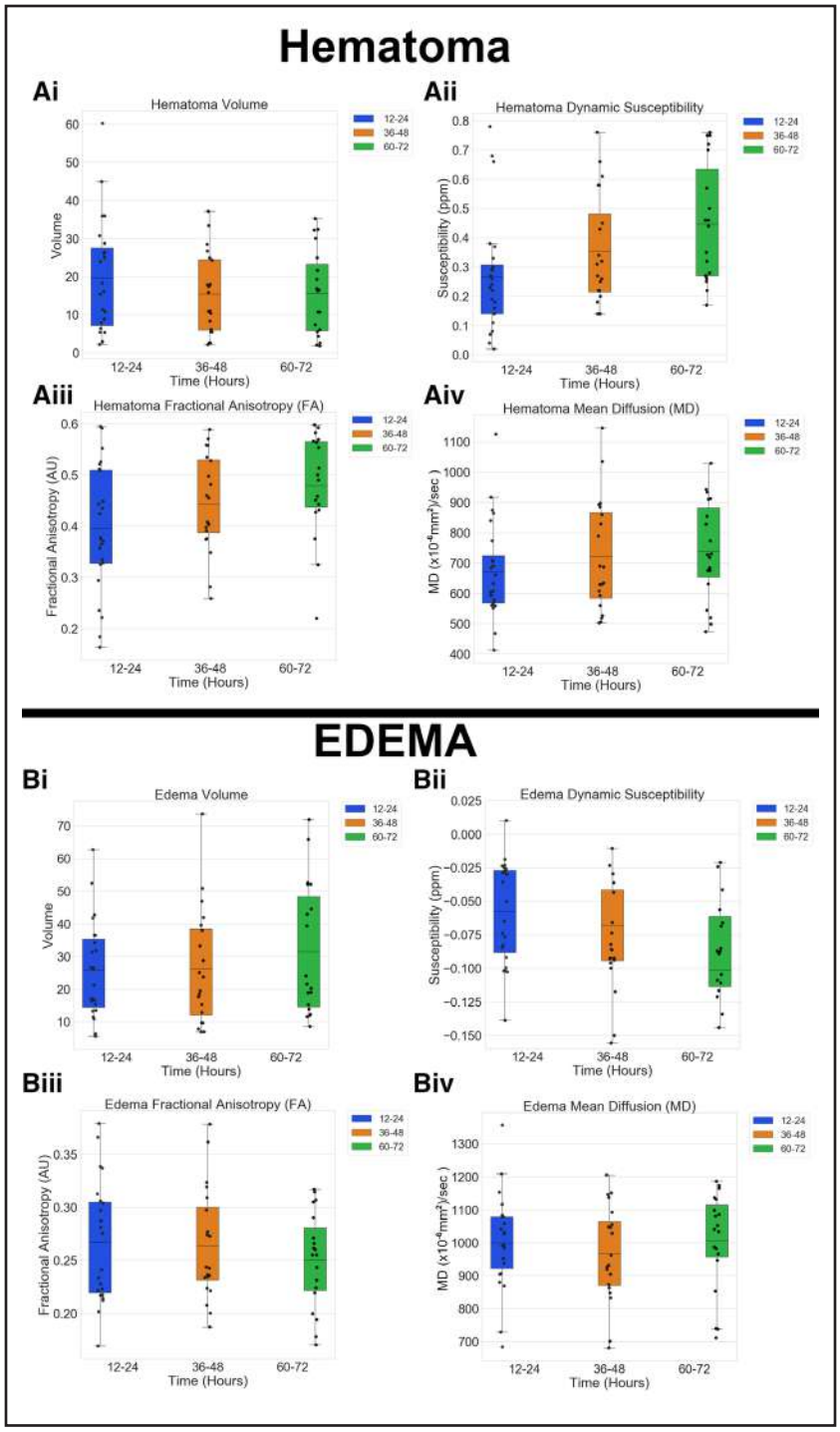

Figure 4. Quantitative changes in imaging metrics are shown using box and whisker plots in the hematoma and perihematomal edema over time. Quantitative temporal changes in the hematoma volume (**Ai**), susceptibility (**Aii**), fractional anisotropy (FA; **Aiii**), and mean diffusivity (MD; **Aiv**), with a significant dynamic increase in the susceptibility ($P<0.0001$) and FA ($P<0.01$). Quantitative temporal changes in the perihematomal edema volume (**Bi**), susceptibility (**Bii**), FA (**Biii**), and MD (**Biv**), with a significant increase in volume ($P<0.05$) and decrease in FA ($P<0.05$). AU indicates arbitrary unit; and ppm, parts per millions.

0.39–2.40]) volumes but not with hematoma susceptibility (coefficient, 0.00066; SE, 0.0065; $P=0.92$ [95% CI, −0.013 to 0.014]). On the other hand, the acute Glasgow Coma Scale at admission exhibited no significant association with hematoma volume, susceptibility, and PHE volume as summarized in Table S1. The serial NIHSS and FM upper extremity scores also had no significant association with hematoma volume, susceptibility, and PHE volume. The association between imaging metrics and clinical assessments is summarized in Table S2.

DISCUSSION

We performed a quantitative MRI study capturing the dynamic changes of blood coagulation during the acute stage of spontaneous ICH. We applied QSM and 2 other neuroimaging markers (FA and MD) to visualize the coagulated blood distribution within the hematoma and to quantify localized coagulation. There are no current methods to measure and visualize clot formation within an intracerebral hematoma in patients. Conventional

CT and MRI have been applied to characterize various stages of hematomas from the acute to chronic stage, but to date, we have no imaging methods that provide direct markers of clot formation. QSM along with high-resolution anatomic images can delineate the heterogeneity of coagulum within the hematoma and differentiate between calcifications and blood, which is not possible using CT alone.

We believe our data, together with the published studies by other groups, support that susceptibility is a noninvasive, quantifiable marker to characterize various stages of hematoma and blood coagulation in ICH.[22,23] The blood phantom image analysis shows a direct relationship between RBC concentration and susceptibility, which is substantiated by the recent use of diffuse reflectance spectroscopy.[27] As compared with the hematoma susceptibility in patients, the blood phantom susceptibilities were significantly lower, and this result is most likely due to either slower formation of fibrin mesh or poor entrapment of RBC and inadequate clot retraction associated with less complete contribution. It is worth pointing out that we noted a significantly higher susceptibility on top of agarose cushion in the tubes. In addition, hypointense signals in susceptibility-weighted imaging have been correlated to RBC-rich clots in ischemic stroke.[26,32] Both histology and in vitro imaging of clots have shown a direct relationship between the clot and RBC concentration.[24,27] The progression of clot formation seen on MRI is directly related to the concentration of deoxyhemoglobin, methemoglobin, and hematocrit within the hematoma, which serve as primary drivers for the observed magnetic susceptibility within a hematoma. The susceptibility within a hematoma also depends on the compartmentalization (intracellular versus extracellular) of methemoglobin. Intracellular methemoglobin induces a significantly higher susceptibility than extracellular sources. This was further corroborated by Bretzner et al,[33] who reported a higher R2* (analogous to susceptibility) in rich coagulated blood as compared with poor coagulated blood.

We went further to show that the observed pockets of high-susceptibility regions seen in MRI within the hematoma are due to coagulated blood and not due to pockets of aggregated RBC. Both the blood and plasma samples with $CaCl_2$ exhibited the presence of a clot, whereas the phantom without $CaCl_2$ remained in a liquid state. Using Martius Scarlet Blue and hematoxylin and eosin stains, the histology analysis of coagulated blood is in line with the previous publication by Fitzgerald et al.[27] The susceptibility data of coagulated blood revealed similar pockets of high susceptibilities as previously seen within the hematoma. Here, the presence of fibrin via Martius Scarlet Blue stain confirmed that those pockets of high susceptibilities were not due to aggregated RBC. Furthermore, the presence of only fibrin in the plasma-rich clot substantiates the significance of fibrin in the clot. In addition, we demonstrated that fresh liquid blood exhibited minimal susceptibility despite the same RBC concentration.

Furthermore, we also found a dynamic increase in diffusion hindrance caused by aggregation of RBC in the hematoma altering the directionality of water molecules, resulting in an increase in FA and a decrease in MD. It should be pointed out that Gupta et al reported an increase in diffusion anisotropy in brain abscesses due to neuroinflammatory molecules. However, they also reported an increase in diffusivity due to abscess, whereas we reported a decrease in hematoma diffusivity due to coagulation.[34] We speculate that the dynamic increase of FA and decrease of MD in the hematoma is not only due to aggregation of RBC but also due to polymerization of fibrin as shown by the histology of plasma clot.[35] In hematoma, both of these elements and platelets are essential for coagulation. Moreover, within the hematoma in the plasma-rich regions (RBC-deficient clot), we would not expect a significant temporal increase in susceptibility but a change in FA and MD.

The increase in susceptibility within the hematoma for up to 72 hours suggests an increase in clot formation over time, but there was variation among patients. Similarly, in blood phantom imaging, Chang et al[23] also found an increase up to 96 hours. Furthermore, in this study, some patients had significantly higher hematoma susceptibility at T1. We suspect the difference was due to a faster rate of coagulation or hematoma age. In previous longitudinal imaging studies of patients with chronic ICH, we did not observe a significant increase in hematoma susceptibility between 1 and 12 months but rather a significant decrease between 3 and 12 months of ictus,[36] which is in line with cross-sectional studies by Chang et al and Champagne et al, who also reported a decrease in hematoma susceptibilities in the later stages of hematoma.

We envision several clinical scenarios where knowledge about the localized rate of coagulation within the hematoma will significantly improve acute management of patients with acute ICH such as (1) reversal/resumption of anticoagulant therapy, (2) a need for continual aggressive hypertension management to control HE, (3) decision of surgical hematoma evacuation, and (4) administration of tPA (tissue-type plasminogen activator) in patients with clotted blood in the ventricles. It is also possible that a hyperacute (within 6 hours of last seen normal) evaluation of QSM may identify patients at risk of HE. In an exploratory analysis, we compared the temporal changes in hematoma volume and susceptibility in patients on oral antithrombotic and no oral antithrombotic. Despite significant sample size limitation and variation, as compared with the no oral antithrombotic group, the oral antithrombotic patients exhibited a relatively lower temporal increase in hematoma susceptibility (0.32±0.1 versus 0.48±0.2 ppm) at 72 hours. These results are presented in Figure S4. For future applications, we envision developing an imaging index of susceptibility along with

 Stroke. 2024;55:1015–1024. DOI: 10.1161/STROKEAHA.123.044343

measurements from FA and MD to define a threshold for coagulation and significant clot formation.

Here, we also provided new temporal information about acute PHE growth over the first 3 days of ICH. Currently, the mechanisms of edema growth in clot formation are not clear. Coagulation initiates blood retraction within the hematoma, which might provide additional extra interstitial space for PHE growth. Furthermore, the temporal increase in PHE susceptibility suggests a trace amount of iron or intact RBCs spread from the hematoma to the surrounding PHE, which is consistent with other studies.[37] Previously, Venkatasubramanian et al[38] reported that PHE growth ranges from as early as 6 hours to as late as 2 weeks depending on several variables. We also showed a continual PHE growth between hyperacute to late acute phase and a trend of association with coagulation, which has been reported in animal studies.[10] Lastly, we showed no HE beyond an average of 18 hours of last seen well, in accordance with prior reports of HE occurring within 6 hours of onset.[39]

There are several limitations to this study. We failed to demonstrate an association between the clinical status and neuroimaging-based quantitative measures. There could be multiple reasons for the failure to observe this association. While NIHSS was strongly associated with the hematoma volume, there were no correlations between NIHSS or FM upper extremity with hematoma susceptibility because of the limitations of these clinical instruments. While FM provides a more precise assessment of motor impairment, it is time-consuming and difficult to perform the test in patients with acute stroke. The majority of the patients were under the heavy influence of medications and so failed to perform the test accurately. In any case, we do not expect significant clinical change within 72 hours of the onset of ICH. It is possible that such an association could have been observed had we scanned the patients over longer periods of time. However, many patients refused our request to continue to participate in this study. The sample size is small, and given the large variability in patient presentation, any association could have been masked the clinical-radiological association. We are currently recruiting more patients and follow them over a longer period of time. We did not image patients with severe ICH because of neurological and cardiovascular instability. The small sample size along with the variability in hematoma size and location was another major limiting factor. Notwithstanding these limitations, in this preliminary study, we believe that it is feasible to map the spatiotemporal evolution of the clot that would have an important role in ICH patient management.

CONCLUSIONS

In conclusion, we present novel imaging measures of coagulation within the hematoma of ICH. We hope our methods will prove useful to examine the clinical relevance of these imaging markers in patient management. For example, clot formation may be beneficial to limit HE and permit earlier resumption of anticoagulants. On the other hand, clot formation may be important for hematoma reabsorption. We hope that these preliminary studies will provide a foundation for a larger study and that imaging markers will be useful in addressing these clinically relevant questions.

ARTICLE INFORMATION

Received June 27, 2023; final revision received December 12, 2023; accepted January 3, 2024.

Affiliations

Institute for Stroke and Cerebrovascular Diseases and Department of Neurology (M.E.H, S.B.B., K.G.S., M.P., S.M.F, I.B., P.H., P.J.Z., F.S.G.C., A.N., M.T., X.Z., J.A., S.I.S.), and Department of Interventional Diagnostic Radiology (K.M.H., P.A.N., C.S.), McGovern Medical School, The University of Texas Health Science Center at Houston (M.E.). Department of Psychiatry, University of Iowa, Iowa City (J.M.). Department of Radiology, Louisiana State University, Shreveport (O.D.A.). Stroke Research and Mobile Stroke Unit, Department of Neurology, Memorial Hermann Hospital, Houston, TX (J.C.G.).

Acknowledgments

The authors thank the members of the magnetic resonance imaging team (Seferino Romo and Raouf Yaqubi) and the nursing staff at Hermann Memorial Hospital. They thank Dr Susan Alderman at The University of Texas Health Science Center at Houston for all their administrative support. They are very grateful to Rhonda Hobbs for providing us with human blood. We appreciate the assistance of Dr Mann in obtaining high-resolution microscopic images.

Sources of Funding

This publication was made possible by funding made available by Texas Legislature to the Lone Star Stroke Research Consortium. Its contents are solely the responsibility of the authors and do not necessarily represent the official views of the State of Texas.

Disclosures

None.

Supplemental Material

Supplemental Materials & Methods
Figures S1–S4
Tables S1–S2

REFERENCES

1. Wilkinson DA, Pandey AS, Thompson BG, Keep RF, Hua Y, Xi G. Injury mechanisms in acute intracerebral hemorrhage. *Neuropharmacology*. 2018;134:240–248. doi: 10.1016/j.neuropharm.2017.09.033
2. Aronowski J, Zhao X. Molecular pathophysiology of cerebral hemorrhage: secondary brain injury. *Stroke*. 2011;42:1781–1786. doi: 10.1161/STROKEAHA.110.596718
3. Bautista W, Adelson PD, Bicher N, Themistocleous M, Tsivgoulis G, Chang JJ. Secondary mechanisms of injury and viable pathophysiological targets in intracerebral hemorrhage. *Ther Adv Neurol Disord*. 2021;14:17562864211049208.doi:10.1177/17562864211049208
4. Garton T, Keep RF, Hua Y, Xi G. Brain iron overload following intracranial haemorrhage. *Stroke Vasc Neurol*. 2016;1:172–184. doi: 10.1136/svn-2016-000042
5. Wu H, Zhang Z, Hu X, Zhao R, Song Y, Ban X, Qi J, Wang J. Dynamic changes of inflammatory markers in brain after hemorrhagic stroke in humans: a postmortem study. *Brain Res*. 2010;1342:111–117. doi: 10.1016/j.brainres.2010.04.033
6. Wu TY, Sharma G, Strbian D, Putaala J, Desmond PM, Tatlisumak T, Davis SM, Meretoja A. Natural history of perihematomal edema and impact on outcome after intracerebral hemorrhage. *Stroke*. 2017;48:873–879. doi: 10.1161/STROKEAHA.116.014416
7. Lv XN, Li ZQ, Deng L, Yang WS, Li YL, Huang YJ, Shen YQ, Xie XF, Li XH, Wang ZJ, et al. Early perihematomal edema expansion: definition, significance,

and association with outcomes after intracerebral hemorrhage. *Oxid Med Cell Longevity*. 2021;2021:6249509. doi: 10.1155/2021/6249509
8. Chen Y, Chen S, Chang J, Wei J, Feng M, Wang R. Perihematomal edema after intracerebral hemorrhage: an update on pathogenesis, risk factors, and therapeutic advances. *Front Immunol*. 2021;12:740632. doi: 10.3389/fimmu.2021.740632
9. Selim M, Norton C. Perihematomal edema: implications for intracerebral hemorrhage research and therapeutic advances. *J Neurosci Res*. 2020;98:212–218. doi: 10.1002/jnr.24372
10. Xi G, Wagner KR, Keep RF, Hua Y, de Courten-Myers GM, Broderick JP, Brott TG, Hoff JT. Role of blood clot formation on early edema development after experimental intracerebral hemorrhage. *Stroke*. 1998;29:2580–2586. doi: 10.1161/01.str.29.12.2580
11. Mould WA, Carhuapoma JR, Muschelli J, Lane K, Morgan TC, McBee NA, Bistran-Hall AJ, Ullman NL, Vespa P, Martin NA, et al; MISTIE Investigators. Minimally invasive surgery plus recombinant tissue-type plasminogen activator for intracerebral hemorrhage evacuation decreases perihematomal edema. *Stroke*. 2013;44:627–634. doi: 10.1161/STROKEAHA.111.000411
12. Kitaoka T, Hua Y, Xi G, Hoff JT, Keep RF. Delayed argatroban treatment reduces edema in a rat model of intracerebral hemorrhage. *Stroke*. 2002;33:3012–3018. doi: 10.1161/01.str.0000037673.17260.1b
13. Lou M, Lieb K, Selim M. The relationship between hematoma iron content and perihematoma edema: an MRI study. *Cerebrovasc Dis*. 2009;27:266–271. doi: 10.1159/000199464
14. Liu C, Li W, Tong KA, Yeom KW, Kuzminski S. Susceptibility-weighted imaging and quantitative susceptibility mapping in the brain. *J Magn Reson Imaging*. 2015;42:23–41. doi: 10.1002/jmri.24768
15. Haacke EM, Liu S, Buch S, Zheng W, Wu D, Ye Y. Quantitative susceptibility mapping: current status and future directions. *Magn Reson Imaging*. 2015;33:1–25. doi: 10.1016/j.mri.2014.09.004
16. Reichenbach JR, Schweser F, Serres B, Deistung A. Quantitative susceptibility mapping: concepts and applications. *Clin Neuroradiol*. 2015;25:225–230. doi: 10.1007/s00062-015-0432-9
17. Sporns PB, Jeibmann A, Minnerup J, Broocks G, Nawabi J, Schön G, Fiehler J, Wildgruber M, Heindel W, Kemmling A, et al. Histological clot composition is associated with preinterventional clot migration in acute stroke patients. *Stroke*. 2019;50:2065–2071. doi: 10.1161/STROKEAHA.118.023314
18. Koneru S, Nogueira RG, Osehobo E, Oprea-Ilies G, Al-Bayati AR, Brinjikji W, Dai D, Haussen DC. Clot composition in retrieved thrombi after mechanical thrombectomy in strokes due to carotid web. *J Neurointerv Surg*. 2021;13:530–533. doi: 10.1136/neurintsurg-2020-017112
19. Bradley WG Jr. MR appearance of hemorrhage in the brain. *Radiology*. 1993;189:15–26. doi: 10.1148/radiology.189.1.8372185
20. Gomori JM, Grossman RI. Mechanisms responsible for the MR appearance and evolution of intracranial hemorrhage. *Radiographics*. 1988;8:427–440. doi: 10.1148/radiographics.8.3.3380989
21. Pauling L, Coryell CD. The magnetic properties and structure of hemoglobin, oxyhemoglobin and carbonmonoxyhemoglobin. *Proc Natl Acad Sci USA*. 1936;22:210–216. doi: 10.1073/pnas.22.4.210
22. Champagne AA, Wen Y, Selim M, Filippidis A, Thomas AJ, Spincemaille P, Wang Y, Soman S. Quantitative susceptibility mapping for staging acute cerebral hemorrhages: comparing the conventional and multiecho complex total field inversion magnetic resonance imaging MR methods. *J Magn Reson Imaging*. 2021;54:1843–1854. doi: 10.1002/jmri.27763
23. Chang S, Zhang J, Liu T, Tsiouris AJ, Shou J, Nguyen T, Leifer D, Wang Y, Kovanlikaya I. Quantitative susceptibility mapping of intracerebral hemorrhages at various stages. *J Magn Reson Imaging*. 2016;44:420–425. doi: 10.1002/jmri.25143
24. Janot K, Oliveira TR, Fromont-Hankard G, Annan M, Filipiak I, Barantin L, Guibon R, Duffy S, Gilvarry M, Cottier JP, et al. Quantitative estimation of thrombus-erythrocytes using MRI. A phantom study with clot analogs and analysis by statistic regression models. *J Neurointerv Surg*. 2020;12:181–185. doi: 10.1136/neurintsurg-2019-014950
25. De A, Sun H, Emery DJ, Butcher KS, Wilman AH. Quantitative susceptibility-weighted imaging in presence of strong susceptibility sources: application to hemorrhage. *Magn Reson Imaging*. 2022;92:224–231. doi: 10.1016/j.mri.2022.06.010
26. Fitzgerald ST, Wang S, Dai D, Douglas A, Kadirvel R, Gounis MJ, Chueh J, Puri AS, Layton KF, Thacker IC, et al. Platelet-rich clots as identified by martius scarlet blue staining are isodense on NCCT. *J Neurointerv Surg*. 2019;11:1145–1149. doi: 10.1136/neurintsurg-2018-014637
27. Skyrman S, Burström G, Aspegren O, Babic D, Lucassen G, Edström E, Arnberg F, Ohlsson M, Mueller M, Elmi-Terander A, et al. Clot composition characterization using diffuse reflectance spectroscopy in acute ischemic stroke. *Biomed Opt Express*. 2022;13:3311–3323. doi: 10.1364/BOE.458445
28. Le Bihan D, Mangin JF, Poupon C, Clark CA, Pappata S, Molko N, Chabriat H. Diffusion tensor imaging: concepts and applications. *J Magn Reson Imaging*. 2001;13:534–546. doi: 10.1002/jmri.1076
29. Verbeke G. Linear mixed models for longitudinal data. In: *Linear Mixed Models in Practice*. Springer; 1997:63–153.
30. Fitzmaurice GM, Laird NM, Ware JH. *Applied Longitudinal Analysis*. John Wiley & Sons; 2012.
31. Rubin DB, Little RJ. *Statistical Analysis With Missing Data*. John Wiley & Sons; 2019.
32. Liebeskind DS, Sanossian N, Yong WH, Starkman S, Tsang MP, Moya AL, Zheng DD, Abolian AM, Kim D, Ali LK, et al. CT and MRI early vessel signs reflect clot composition in acute stroke. *Stroke*. 2011;42:1237–1243. doi: 10.1161/STROKEAHA.110.605576
33. Bretzner M, Lopes R, McCarthy R, Corseaux D, Auger F, Gunning G, Beauval N, Bongiovanni A, Tardivel M, Cordonnier C, et al. Texture parameters of R2* maps are correlated with iron concentration and red blood cells count in clot analogs: a 7-T micro-MRI study. *J Neuroradiol*. 2020;47:306–311. doi: 10.1016/j.neurad.2019.10.004
34. Gupta RK, Nath K, Prasad A, Prasad KN, Husain M, Rathore RK, Husain N, Srivastava C, Khetan P, Trivedi R, et al. In vivo demonstration of neuroinflammatory molecule expression in brain abscess with diffusion tensor imaging. *AJNR Am J Neuroradiol*. 2008;29:326–332. doi: 10.3174/ajnr.A0826
35. Mereuta OM, Rossi R, Douglas A, Gil SM, Fitzgerald S, Pandit A, McCarthy R, Gilvarry M, Ceder E, Dunker D, et al. characterization of the 'white' appearing clots that cause acute ischemic stroke. *J Stroke Cerebrovasc Dis*. 2021;30:106127. doi: 10.1016/j.jstrokecerebrovasdis.2021.106127
36. Haque ME, Boren SB, Arevalo OD, Gupta R, George S, Parekh MA, Zhao X, Aronowski J, Savitz SI. Longitudinal, quantitative, multimodal MRI evaluation of patients with intracerebral hemorrhage over the first year. *Front Neurol*. 2021;12:764718. doi: 10.3389/fneur.2021.764718
37. Wei J, Novakovic N, Chenevert TL, Xi G, Keep RF, Pandey AS, Chaudhary N. Perihematomal brain tissue iron concentration measurement by MRI in patients with intracerebral hemorrhage. *CNS Neurosci Ther*. 2020;26:896–901. doi: 10.1111/cns.13395
38. Venkatasubramanian C, Mlynash M, Finley-Caulfield A, Eyngorn I, Kalimuthu R, Snider RW, Wijman CA. Natural history of perihematomal edema after intracerebral hemorrhage measured by serial magnetic resonance imaging. *Stroke*. 2011;42:73–80. doi: 10.1161/STROKEAHA.110.590646
39. Brouwers HB, Greenberg SM. Hematoma expansion following acute intracerebral hemorrhage. *Cerebrovasc Dis*. 2013;35:195–201. doi: 10.1159/000346599